Effects of extrusion variables on temperature distribution in axisymmetric extrusion process

J.S. Ajiboye[a,*], M.B. Adeyemi[b]

[a]Department of Mechanical Engineering, University of Lagos, Lagos, Nigeria
[b]Department of Mechanical Engineering, University of Ilorin, Ilorin, Nigeria

Abstract

A numerical method was developed to simulate the non-steady-state temperature distributions during forward extrusion process. The velocity, strain rates, and strain fields within the deformation zones during extrusion were obtained, using upper bound method of analysis to obtain internal heat generations coupled to the necessary heat transfer conduction equations. The computer program written in C++ language essentially simulates the extrusion process and takes into account extrusion variables such as material properties, friction conditions, extrusion velocity, extrusion ratio, die preheat temperature, billet height, percentage reduction in area, and die land length. The effects of billet height and percentage reduction in area on the temperature distributions within the dead metal zone give good agreements with experimental results. It is found that the higher the billet's heights and higher the percentages reduction in areas, the higher the temperature rises during the extrusion process. The die land zone shows increasing temperature rise with increasing friction coefficient, while increasing friction coefficient has no effect on the dead zone temperature. Also, increasing speed of deformation shows an increasing dead zone temperature rise than a more gradual die land temperature rise. It can be stated that the extrusion temperature increases proportionally to the increase of the container temperature.
© 2007 Elsevier Ltd. All rights reserved.

Keywords: Billet height; % reduction in area; Dead metal zone; Die land zone; Temperature distribution; Ram travel

1. Introduction

In metalworking, the essential features are the occurrence of extremely high pressures and temperatures during the process, this being due to the constraints imposed by rigid tools. The high pressure and temperature may increase ductility of the material, which in turn enables large deformations to take place in one operation without the material cracking. When a material is plastically deformed, a very large part of the work expended appears as heat energy. The temperature generated reduces the flow stress of the material, which consequently makes the energy required for deformation to be reduced. Farren and Taylor [1] showed that for a heavily deformed metal about 90% of the deformation energy is converted into heat. Altan and Kobayashi [2] found that, for large reductions and

commercial speeds used in extrusion, temperature increases of several hundred degrees may be involved. They reported that about 95% of the mechanical work of deformation is converted into heat. Some of the heat is conducted away by the tools or lost to the atmosphere, but a portion remains to increase the temperature of the workpiece.

Akeret [3] has analyzed the transient heat transfer and temperature distribution in direct extrusion, using a simple numerical method which assumes that the billet is composed of cells of constant temperature. In order to avoid too high extrusion load, exact temperature and speed conditions must be kept. These conditions are specially important in order to attain required and homogeneous properties both along and in the cross-section of the extrude. To provide the ideal conditions for the process, such parameters should be chosen that may guarantee the isothermal process, i.e. the temperature of the extrusion remains on the same level throughout the whole process. To obtain this, we need to determine the effect of the main

---

*Corresponding author.

E-mail address: joesehinde@yahoo.com (J.S. Ajiboye).

Nomenclature

A_f	final extrude area
A_o	original billet area
A_o/A_f	extrusion ratio
Bi	(Biot number) $= h^* \Delta l / k$
C_n	heat capacity of billet or tooling materials
CT	container temperature
F, G	factors used to adjust nodes at irregular boundary $(0 < F, G \leqslant 1)$
F_o	(Fourier number) $= \alpha \beta / \Delta l^2$
F_{o_1}	Fourier number for the working material prior to deformation
F_{o_2}	Fourier number of deforming billet
F_{o_3}	Fourier number of the extrude
F_{o_4}	Fourier number of die material
F_{o_5}	Fourier number of container material
F_{o_6}	Fourier number of pad material
H^*	enthalpy
H_o	original billet height
h^*	convective heat transfer coefficient
J^*	total upper bound on power
k_n	thermal conductivity of billet and tooling materials
m	friction coefficient
R^*	outer radius of container
R	% reduction in area
r_o	original billet radius
r_f	extrude radius
$r_s(\varphi, y)$	function defining the shape of die geometry
$\varsigma(\varphi)$	shape of exit cross-section
S	constant annular surface area between two axial lines, m^2
t	time
t_c	thickness of the container
T_o	initial temperature
T_i	$(i = 1, 2, \ldots, 6)$ temperature field
T_∞	ambient temperature (amb)
ΔT	temperature rise
ΔT_j	temperature rise due to velocity jump at boundaries of velocity discontinuities
ΔT_1	temperature rise in the undeformed billet
ΔT_2	temperature rise due to plastic deformation
ΔT_{1-5}	temperature rise due to boundary friction at billet/container interface
ΔT_3	temperature rise due to boundary friction at extrude/die land interface
ΔT_{2-4}	temperature rise due to boundary friction at deforming billet/die interface
Δl	mesh size
v_o, v_z	steady punch velocity
V_r, V_y, V_φ	velocity components
ΔV	resultant velocity
$\dot{W}_f$	frictional energy losses
$\dot{W}_i$	internal power of deformation
$\dot{W}_s$	shear power loss
x	die land length
y_1	die length

Greek alphabets

ρ	density
$\dot{\varepsilon}_{ij}\dot{\varepsilon}_{ij}$	strain rate components
σ_o	flow stress of the billet
β	spatial time step
$\omega\,(\varphi, y)$	angular velocity
Γ_s	surfaces of velocity discontinuities
$\varphi_f(y)$	function defining the boundary of plastic zone
τ	frictional shear stress
α	thermal diffusivity $(k/\rho C)$

extrusion parameters on the extrusion temperature, temperature of the dead zone, and the emergent or die land zone. Each of these zones influences essentially the metal flow behaviour in the main deformation zone, and the manner of the temperature changes of the extrusion process. To properly analyze the power requirements for metalworking processes, the flow stress, speed, and deformation temperature must be known. The major difficulty, of course, is that these basic variables—flow stress, speed, and deformation temperature—are closely interrelated and any analysis must consider simultaneously all three variables. Research work has already been conducted to determine how the emergent temperatures are related to extrusion variables. Tanner and Johnson [4], in their work on the temperature distributions in the die zone during fast extrusion operations, concluded that for lead and steel, if the speed of extrusion was greater than 71.12 mm/s, then the heat conduction back to the unextruded billet was found to be negligible. Temperature

changes in the material during extrusion can be predicted when information is available regarding the strain, strain rate distributions, and the thermal properties of the billet and tool materials. Singer and Al-Samarrai [5] attempted to predict the emergent temperature of the product by assuming a simple model in which all deformation takes place, as the metal crosses the exit plane of the die. In their calculations of the heat generation, they considered only axial heat flow, neglecting the container friction. Johnson and Kudo [6] neglected the die material friction and assumed an ideal plastic material for their calculations of the adiabatic temperature increase in an axisymmetric extrusion based on an admissible velocity field.

The present work gives generalized temperature distributions at any positions, arising from axisymmetric extrusion process by generalizing the shapes of the die profiles and analyzing, deforming, undeforming, and extruding zones. The temperature distributions arising from any configurations, complex or simple shapes sections can be tracked,

using the present numerical simulations based on upper bound analysis, involving various zones during extrusion process. It is obvious that the temperature distributions in the material during extrusion depend on several factors such as material properties, friction conditions, ram velocity, extrusion ratio, preheat temperature, billet height, and die land length, which are taken into account in the present analyses. Effects of extrusion speed, percentage reduction in area, container/tool temperature, initial billet temperature, and friction coefficient for circular die openings are analyzed in the present work and comparison made with existing results in literatures.

2. Theoretical analysis

2.1. Velocity fields and upper bound method for internal heat generation

Fig. 1 shows the schematic diagram of the shape and dimension of the linearly converging die in cylindrical coordinate system used for the present numerical calculations. The kinematically admissible velocity fields with discontinuities formulated by Kiuchi et al. [7] are used for
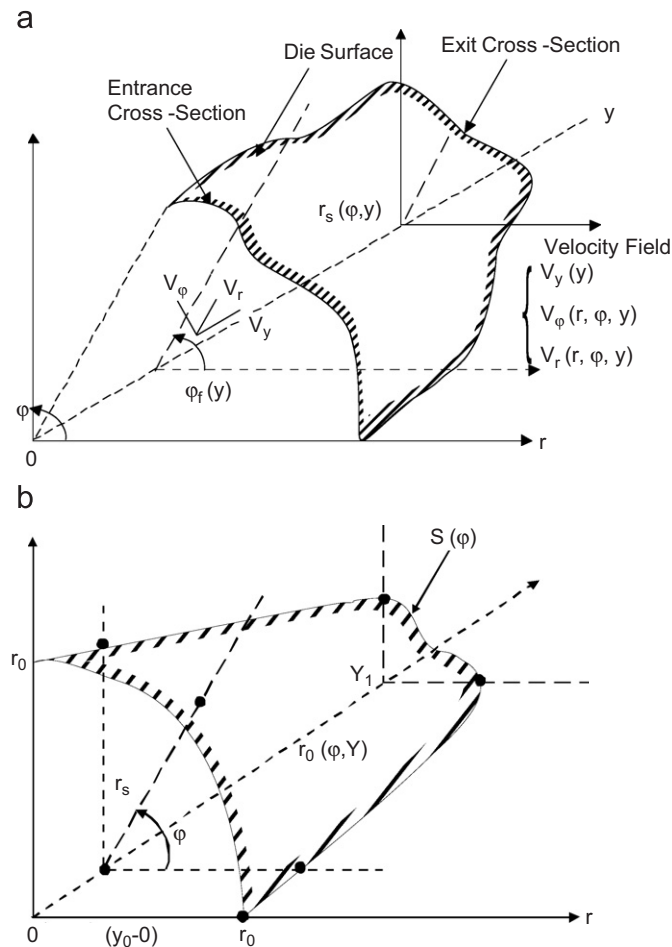

Fig. 1. (a) Schematic diagram of the die surface in cylindrical co-ordinate and (b) shape and dimension of linearly converging die used in numerical calculation.

calculating the strain rates in the deformation zone. The method used in the present work for determining the non-steady-state temperature distributions in extrusion requires a steady-state-kinematically admissible velocity fields from where strain rate distributions, powers of plastic deformation/unit volume, $\dot{W}_i$, the boundary friction, $\dot{W}_f$, and power due to velocity discontinuities, $\dot{W}_s$, are evaluated using upper bound approach. A mathematical model for simulating extrusion must represent the geometry of the die closely, particularly in the regions with the highest gradients in flow velocity and temperature.

It is assumed that the material is homogeneous and friction coefficient is constant over the contact surfaces.

For circular billet, the shape of the die surface, $r_s(\varphi, y)$ is approximated as

$$r_s(\varphi, y) = \frac{\varsigma(\varphi) - r_o}{y_1} y + r_o, \tag{1}$$

where r_o is the radius of the round billet and y_1 is the length of the die. By using Eq. (1), and the function $r_s(\varphi, y)$, all the strain rate components and the total powers of deformation can be calculated.

2.1.1. Assumptions
The following assumptions [7,8] are used:

(i) the longitudinal velocity, V_y, is uniform at each cross-section of the material in the die and is equal to inlet velocity denoted by V_o at the entry;
(ii) the Von-Mises yield criterion is assumed to be applicable;
(iii) the rotational velocity component $V_\varphi(r, \varphi, y)$ is expressed as a product of two functions as follows: $V\varphi(r, \varphi, y) = r.\omega(\varphi, y)$.

The generalized formulae of the kinematically admissible velocity field can be formulated as follows:

From the continuity equation we have

$$\dot{\varepsilon}_r + \dot{\varepsilon}_\varphi + \dot{\varepsilon}_y = 0, \tag{2}$$

that is

$$\frac{\partial V_r(r, \varphi, y)}{\partial r} + \frac{1}{r} V_r(r, \varphi, y) + \frac{\partial V_y(r, \varphi, y)}{\partial y}$$

$$+ \frac{1}{r} \frac{\partial V\varphi(r, \varphi, y)}{\partial \varphi} = 0. \tag{3}$$

From here, the velocity fields' equations are derived as

$$V_y(v) = \frac{V_0 \int_0^{\varphi(0)} r_s^2(\varphi, 0)\, d\varphi}{\int_0^{\varphi(y)} r_s^2(\varphi, y)\, d\varphi}, \tag{4}$$

$$V_r(r, \varphi, y) = \frac{1}{r} \int_0^r r \left[\frac{dV_y(y)}{dy} + \frac{1}{r} \frac{\partial V_\varphi(r, \varphi, y)}{\partial \phi} \right] dr, \tag{5}$$

$$V_\varphi(r, \varphi, y) = \frac{r}{r_s^2(\varphi, y)} \int_0^\varphi \frac{\partial}{\partial y} \left[V_y(y) r_s^2(\varphi, y) \right] d\varphi. \tag{6}$$

2.1.2. Strain rates and powers of deformations

The strain rate components [7] are defined based on kinematically admissible velocity fields of Eqs. (4), (5) and (6) as follows:

$$\dot{\varepsilon}_{rr}(\varphi,y) = \frac{1}{2}\left[\frac{\partial \omega(\varphi,y)}{\partial \varphi} + \frac{\partial V_y(y)}{\partial y}\right], \tag{7}$$

$$\dot{\varepsilon}_{\varphi\varphi}(\varphi,y) = \frac{1}{2}\left[\frac{\partial \omega(\varphi,y)}{\partial \varphi} - \frac{\partial V_y(y)}{\partial y}\right], \tag{8}$$

$$\dot{\varepsilon}_{yy}(y) = \frac{\partial V_y(y)}{\partial y}, \tag{9}$$

$$\dot{\varepsilon}_{r\varphi}(\varphi,y) = -\frac{1}{4}\frac{\partial \omega(\varphi,y)}{\partial^2 \varphi}, \tag{10}$$

$$\dot{\varepsilon}_{\varphi y}(r,\varphi,y) = \frac{r}{2}\frac{\partial \omega(\varphi,y)}{\partial y}, \tag{11}$$

$$\dot{\varepsilon}_{yr}(r,\varphi,y) = \frac{r}{4}\left[\frac{\partial^2 \omega(\varphi,y)}{\partial y \partial \varphi} + \frac{\partial^2 Vy}{\partial y^2}\right]. \tag{12}$$

2.1.3. Upper bound solution

The upper bound formulation is described as follows:

$$J^* = \frac{2}{\sqrt{3}}\sigma_o \int_v \sqrt{\frac{1}{2}\dot{\varepsilon}_{ij}\dot{\varepsilon}_{ij}}\,\mathrm{d}V + \tau \int_{\Gamma_s}|\Delta V|\Gamma_s\mathrm{d}S$$
$$+ m\tau \int_s |\Delta V|\mathrm{d}S. \tag{13}$$

The first term of Eq. (13) represents the internal powers dissipated for the deformed zone, second term represents shear losses, and the third term represents frictional losses on the tool–workpiece interface. σ_o is the flow stress of material, ε_{ij} the derived strain rate tensor, $|\Delta V|$ is the velocity discontinuity over the shear surfaces, and m the constant friction factor.

The terms in Eq. (13) can be expanded as follows:

$$\dot{W}_i = \sigma_o \int\int\int \sqrt{\frac{2}{3}\left(\dot{\varepsilon}_{rr}^2 + \dot{\varepsilon}_{\varphi\varphi}^2 + \dot{\varepsilon}_{yy}^2 + 2\left\{\dot{\varepsilon}_{r\varphi}^2 + \dot{\varepsilon}_{y\varphi}^2 + \dot{\varepsilon}_{yr}^2\right\}\right)}$$
$$\times r\,\mathrm{d}r\,\mathrm{d}\varphi\,\mathrm{d}y. \tag{14}$$

The shear power loss $\dot{W}_S$, is given by

$$\dot{W}_S = \int_{\Gamma_s} \frac{\bar{\sigma}_o}{\sqrt{3}}(\Delta V)\Gamma_s\,\mathrm{d}s, \tag{15}$$

where Γ_s are boundaries of velocity discontinuity at exit, entry including singular points and

$$(\Delta V)\Gamma_s = \sqrt{\left[V_\varphi^2(r,\varphi,y^*) + V_r^2(r,\varphi,y^*)\right]}, \tag{16}$$

where y^* is the y-coordinate denoting the entrance and exit.

The relative slip on the internal boundaries of velocity discontinuity is expressed by

$$\Delta V_r = -\frac{r}{2}\left[\frac{\partial \omega(\varphi+0,y)}{\partial \varphi} - \frac{\partial \omega(\varphi-0,y)}{\partial \varphi}\right]. \tag{17}$$

The frictional power dissipated at the tool/material interface is given by

$$\dot{W}_{F_2} = \frac{m\sigma_0}{\sqrt{3}}\int_0^{r_o}\int_0^{2\pi}|V_r|r\,\mathrm{d}\varphi\,\mathrm{d}y,$$

where V_r is the radial velocity, given as

$$V_r(\varphi,r,y) = -\frac{r}{2}\left[\frac{\partial V_y(y)}{\partial y} + \frac{\partial \omega(\varphi,y)}{\partial \varphi}\right]. \tag{18}$$

A computer program written in C++ language was used to evaluate the above volume and area integrals to give the powers of plastic deformation, $\dot{W}_i$, the frictional power, $\dot{W}_f$, and the power due to velocity discontinuities at the boundaries, $\dot{W}_s$. These energy components are then converted to temperatures increase due to boundary friction at undeformed/container interface (ΔT_{1-5}) and extrude/die land interface (ΔT_6), plastic deformation (ΔT_2), and due to velocity discontinuities (ΔT_j). The program developed is of a general form and can be used for extrusion under varying operating parameters.

2.2. Heat transfer equations and boundary conditions analyses within each zone in extrusion process

2.2.1. Assumptions

To formulate [9] the governing equations for the heat transfer/conduction during extrusion process, some assumptions are necessary: The basic assumptions are:

1. the material is homogeneous and isotropic;
2. for the deforming billet it is assumed that heat transfer is by conduction only;
3. it is assumed that the workpiece is in perfect contact with the container and die throughout the extrusion operation, so that no resistance to heat flow occurs at the interfaces;
4. it is assumed that the energy generation is due to deformation of material and boundary friction along the container wall during compression and extrusion stages, resulting to temperature changes.

During extrusion, heat is generated by deformation of the material, shearing at the deformation-zone boundaries and friction at the tool–material interfaces. Some of the heat generated is transported with the deformed material, some is transmitted to the punch, container, and die, and some increases the temperature of the billet. This complex problem, involving simultaneous heat generation, transportation, and conduction was simulated with a numerical method of solution. This finite difference method considers the effects of internal heat generation, conduction, and mass transfer on the basis of local temperatures and strain rate in each time increment for the solution. The sketch below represents extrusion chamber of a linearly converging die with various points or zones where heat generation and conduction occur simultaneously (Fig. 2).
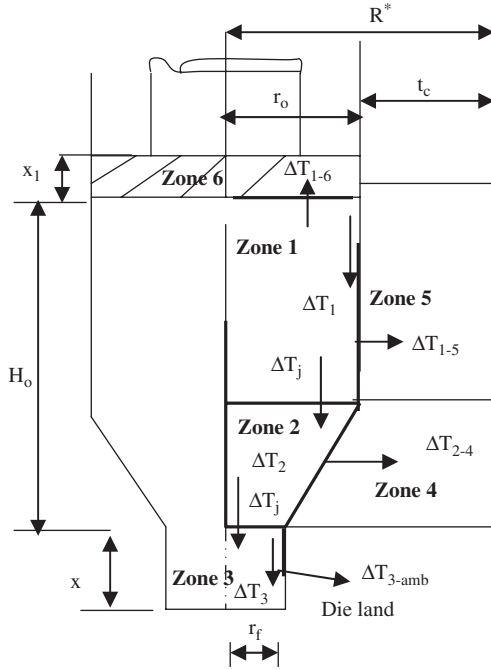
Fig. 2. Idealized extrusion chamber showing various zones of extrusion process. *Zone* 1 is billet prior to deformation. *Zone* 2 is deforming billet. *Zone* 3 is the extrude passing through the die land length generating frictional heat. *Zone* 4 is the die. *Zone* 5 is the container receiving some heat due to temperature gradient existing between it and the warm billet. *Zone* 6 is the punch head or pad. As the punch descends, the extrusion takes place, and heat is generated by deformation in the material and by boundary friction at the tool–material interface.

2.2.2. Heat transfer zones and analyses

2.2.2.1. Zone 1: Conduction heat transfer equation prior to deformation. The heat transfer equation prior to the commencement of deformation is expressed as

$$\rho_1 C_1 \left[\frac{\partial T_1}{\partial t} + V_z \frac{\partial T_1}{\partial z} \right]$$
$$= k_1 \left[\frac{\partial^2 T_1}{\partial r^2} + \frac{1}{r} \frac{\partial T_1}{\partial r} + \frac{\partial^2 T_1}{\partial z^2} \right] + \Delta T_{1-5},$$
$$0 \leqslant z_j \leqslant V_z t, \ \ 0 \leqslant r_i \leqslant r_o, \ \ t = 0, \ \ T(r,z) = T_o;$$
$$\frac{k_1 \partial T}{\partial r} = 0 \text{ at } r = 0, \tag{19}$$

where ΔT_{1-5} = heat generated due to boundary friction force over the container surface.

Energy balance at the interfaces with zone 5

(i) Undeformed billet/container interface (boundary):

$$k_1 \frac{\partial T_1}{\partial r} + \rho_1 C_1 \frac{\Delta l}{2} \frac{\partial T_1}{\partial t} + \Delta T_{1-5}$$
$$= k_5 \frac{\partial T_5}{\partial r} + \rho_5 C_5 \frac{\Delta l}{2} \frac{\partial T_5}{\partial t},$$
$$0 \leqslant z_j \leqslant V_z t \text{ at } r = r_o; \ \ \Delta l \text{ is the mesh size.} \tag{20}$$

(ii) Undeformed billet/pad interface:

$$k_1 \frac{\partial T_1}{\partial z} + \rho_1 C_1 \frac{\Delta l}{2} \frac{\partial T_1}{\partial t} + \Delta T_{1-6}$$
$$= \rho_6 C_6 \frac{\Delta l}{2} \frac{\partial T_6}{\partial t} + k_6 \frac{\partial T_6}{\partial z},$$
$$0 \leqslant r_i \leqslant r_o; \ \ H_o \leqslant z_j \leqslant H_o - V_z t,$$
$$t = 0, \ \ T(z,r) = T_o. \tag{21}$$

ΔT_{1-6} = heat generated due to friction force between billet/pad interface.

2.2.2.2. Zone 2: Heat transfer in deforming billet. The conduction heat transfer equation within the deforming billet is expressed as

$$\rho_2 C_2 \left[\frac{\partial T_2}{\partial t} + V_z \frac{\partial T_2}{\partial z} \right]$$
$$= k_2 \left[\frac{\partial^2 T_2}{\partial r^2} + \frac{1}{r} \frac{\partial T_2}{\partial r} + \frac{\partial^2 T_2}{\partial z^2} \right] + \Delta T_2,$$
$$0 \leqslant r_i \leqslant r_o, \ \ 0 \leqslant z_j \leqslant - V_z t, \ \ t = 0, \ \ T(r,z) = T_o, \tag{22}$$

where ΔT_2 = the energy generated due to the work of plastic deformation per unit volume.

Energy balance at the interfaces with zone 4

(i) Deforming billet/undeformed billet interface:

$$k_1 \frac{\partial T_1}{\partial z} + \rho_1 C_1 \frac{\Delta l}{2} \frac{\partial T_1}{\partial t} + \Delta T_j$$
$$= k_2 \frac{\partial T_2}{\partial z} + \rho_2 C_2 \frac{\Delta l}{2} \frac{\partial T_2}{\partial t},$$
$$0 \leqslant r_i \leqslant r_o \text{ at } z = 0; \ \ t = 0, \ \ T(r,z) = T_o. \tag{23}$$

(ii) Deforming billet/extrude interface:

$$k_2 \frac{\partial T_2}{\partial z} + \rho_2 C_2 \frac{\Delta l}{2} \frac{\partial T_2}{\partial t} + \Delta T_j$$
$$= k_3 \frac{\partial T_3}{\partial z} + \rho_3 C_3 \frac{\Delta l}{2} \frac{\partial T_3}{\partial t},$$
$$0 \leqslant r_i \leqslant r_o \text{ at } z_j = - V_z t,$$
$$t = 0, \ \ T(r,z) = T_o. \tag{24}$$

Irregular boundaries in the deforming billet

At the irregular boundaries, where nodes fall on boundary between the deforming billet and the die, the energy balance between the deforming billet and the die is given by the next Eq. (25).

(iii) Energy balance at deforming/die interface
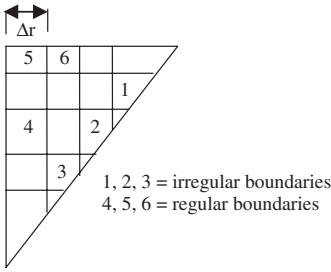
Deforming billet/die interface:

$$k_2 \frac{\partial T_2}{\partial r} + \rho_2 C_2 \frac{\Delta l}{2} \frac{\partial T_2}{\partial t} + \Delta T_{2-4}$$

$$= k_4 \frac{\partial T_4}{\partial r} + \rho_4 C_4 \frac{\Delta l}{2} \frac{\partial T_4}{\partial t},$$

$$0 \leqslant r_i \leqslant - V_z t \text{ at } r = r_f, \tag{25}$$

where r_i varies between r_o and r_f. This can be better modified by using the profile of constant strain rate (CSR) die in terms of the axial distance (y_1) and extrusion ratio $\lambda = (r_o^2/r_f^2)$ is given [10] as

$$r(y) = \sqrt{\frac{r_o^2}{[(\lambda - 1)y/y_1 + 1]}}, \qquad \qquad \tag{26}$$

1, 2, 3 = irregular boundaries
4, 5, 6 = regular boundaries

2.2.2.3. Zone 3: Heat transfer in extruded section. The conduction heat transfer equation in the extruded billet is expressed as

$$\rho_3 C_3 \left[\frac{\partial T_3}{\partial t} + V_z \frac{\partial T_3}{\partial z} \right]$$
$$= k_3 \left[\frac{\partial^2 T_3}{\partial r^2} + \frac{1}{r} \frac{\partial T_3}{\partial r} + \frac{\partial^2 T_3}{\partial z^2} \right] + \Delta T_3,$$

$$0 \leqslant r_i \leqslant r_f : V_z t \leqslant z_j \leqslant - V_e t, \quad t = 0,$$
$$T(r,z) = T_o. \tag{27}$$

where ΔT_3 = heat generated due to boundary friction at the die land–extrude interface.

Energy balance with the interface:
    Extruded billet/ambient interface:

$$\rho_3 C_3 \frac{\Delta l}{2} \frac{\partial T_3}{\partial t} + k_3 \frac{\partial T_3}{\partial r} = H^*(T_{i,j}^i - T_\infty),$$
$$t = 0, \quad T(r,z) = T_o \text{ at } r = r_f. \tag{28}$$

2.2.2.4. Zone 4: Conduction heat transfer equation within the die. The conduction heat transfer equation within the die is expressed as

$$\rho_4 C_4 \frac{\partial T_4}{\partial t} = k_4 \left[\frac{\partial^2 T_4}{\partial r^2} + \frac{1}{r} \frac{\partial T_4}{\partial r} + \frac{\partial^2 T_4}{\partial z^2} \right],$$
$$0 \leqslant zj \leqslant v_z t; \quad R \leqslant r_i \leqslant t_c; \quad t = 0, \quad T(r,z) = T_o. \tag{29}$$

The energy balance between the die and the ambient air is

$$K_4 \frac{\partial T_4}{\partial r} + \rho_4 C_4 \frac{\Delta l}{2} \frac{\partial T_4}{\partial t} = H^*(T_{i,j}^i - T_\infty),$$
$$0 \leqslant zi \leqslant H_o - v_z t \text{ at } R; \quad t = 0, \quad T(r,z) = T_o. \tag{30}$$

2.2.2.5. Zone 5: Heat transfer in the container. The conduction heat transfer equation in the container is

expressed as

$$\rho_5 C_5 \frac{\partial T_5}{\partial t} = k_3 \left[\frac{\partial^2 T_5}{\partial r^2} + \frac{1}{r} \frac{\partial T_5}{\partial r} + \frac{\partial^2 T_5}{\partial z^2} \right],$$
$$0 \leqslant z_i \leqslant V_z t; \quad r_o \leqslant r_i \leqslant t_c + r_o; \quad t = 0, \quad T(r,z) = T_o. \tag{31}$$

The energy balance between the container and the ambient is

$$k_5 \frac{\partial T_5}{\partial r} + \rho_5 C_5 \frac{\Delta l}{2} \frac{\partial T_5}{\partial t} = H^*(T_{i,j}^i - T_\infty),$$
$$0 \leqslant z_i \leqslant H_o - V_z t \text{ at } r = R^*;$$
$$t = 0, \quad T(r,z) = T_o. \tag{32}$$

2.2.2.6. Zone 6: Heat transfer in the punch. The conduction heat transfer equation in the extruded billet is expressed as,

$$\rho_6 C_6 \frac{\partial T_6}{\partial t} = k_6 \left[\frac{\partial^2 T_6}{\partial r^2} + \frac{1}{r} \frac{\partial T_6}{\partial r} + \frac{\partial^2 T_6}{\partial z^2} \right],$$
$$H_o \leqslant z_j \leqslant - x_1; \quad 0 \leqslant r_i \leqslant r_o; \quad t = 0, \quad T(r,z) = T_o, \tag{33}$$

where x_1 is the pad thickness.

Energy balance with the ambient
    Pad or punch/ ambient interface

$$K_6 \frac{\partial T_6}{\partial z} + \rho_6 C_6 \frac{\Delta l}{2} \frac{\partial T_6}{\partial t} = H^*(T_{i,j}^i - T_\infty),$$
$$0 \leqslant r_i \leqslant r_o; \quad x_1 \leqslant z_j \leqslant H_o; \quad t = 0, \quad T(r,z) = T_o, \tag{34}$$

where x_1 is the pad thickness.

2.3. Method of numerical solutions

The solutions to the above governing equations and energy balances (19)–(34) at their boundaries conditions are expressed in the finite difference forms as follows [11].

2.3.1. Finite difference forms of each zone
    Zone 1: Heat transfer equation in undeformed region
    The coordinates of the node (i,j) are simply $h = r = i. \Delta r$ and $z = j. \Delta z$, and the temperature at the node (i,j) is denoted by $T_{i,j}$. Now, the finite difference approximation of the partial derivatives $\partial T/\partial t$ that appears in the differential equations of transient problems is $T_{i,j}^{n+1} - T_{i,j}^n/\beta$, where $T_{i,j}^n$ and $T_{i,j}^{n+1}$ are the temperatures of node i,j at times $t_n = n\beta$ and $t_{n+1} = (n+1)\beta$, respectively. The new temperature $T_{i,j}^{n+1}$ is determined from previous temperature $T_{i,j}^n$. In transient problems, the superscript n is used as the index or counter of time steps, with $n = 0$ corresponding to the specified initial conditions.

Replacing the partial differential form of Eq. (19) with the equivalent finite difference form, we have

$$\rho_1 C_1 \left[\frac{(T_{i,j}^{n+1} - T_{i,j}^n)}{\beta} + V_z \frac{(T_{i,j+1}^n - T_{i,j}^n)}{\Delta z} \right],$$
$$= k_1 \left[\frac{(T_{i+1,j}^n - 2T_{i,j}^n + T_{i-i,j}^n)}{\Delta r^2} \right]$$

$$+ \frac{1}{r} \frac{(T_{i+1,j}^n - T_{i,j}^n)}{\Delta r}$$
$$+ \frac{(T_{i,j+1}^n - 2T_{i,j}^n + T_{i,j-1}^n)}{\Delta z^2} + \Delta T_1, \qquad (35a)$$

which simplified to

$$T_{i,j}^{n+1} = \frac{\alpha_3 \beta}{\Delta l^2}(T_{i+1,j}^n - 2T_{i,j}^n + T_{i-i,j}^n)$$
$$+ \frac{\alpha_3 \beta}{r} \frac{(T_{i+1,j}^n - T_{i,j}^n)}{\Delta l} + \frac{\alpha_3 \beta}{\Delta l^2}$$
$$\times (T_{i,j+1}^n - 2T_{i,j}^n + T_{i,j-1}^n)$$
$$+ \Delta T_1 - V_z \frac{(T_{i,j+1}^n - T_{i,j}^n)}{\Delta l} + T_{i,j}^n. \qquad (35b)$$

The above Eq. (35b) was rearranged, with $r = i\Delta l$, to give a typical temperature distribution at point i,j (see Fig. 3) within the undeformed billet as

$$T_{i,j}^{n+1} = F_o(1 + \frac{1}{2i})T_{i+1,j}^n + F_o(1 - \frac{1}{2i})T_{i-1,j}^n,$$
$$+ (1 - 4F_o)T_{i,j}^n + (F_o - \frac{V_o \beta}{2\Delta l})T_{i,j+1}^n,$$
$$+ (F_o + \frac{V_o \beta}{2\Delta l})T_{i,j-1}^n + \Delta T_2. \qquad (35)$$

Now, replacing the partial differential form of Eqs. (20) and (21), representing the energy balances between the undeformed billet/pad and the undeformed billet/container interfaces, with the equivalent finite difference form to give the next expressions representing the temperature distributions at respective interfaces as

$$T_{i,j}^{n+1} = \left\{ \left(\frac{k_6 - k_1}{k_1}\right) \left\langle \frac{2k_1 F_{o_1} F_{o_6}}{(k_1 F_{o_6} - k_6 F_{o_1})} \right\rangle \right\} T_{i+1,j}^n$$
$$+ \left\{ 1 + \left(\frac{k_1 - k_6}{k_1}\right) \left\langle \frac{2k_1 F_{o_1} F_{o_6}}{(k_1 F_{o_6} - k_6 F_{o_1})} \right\rangle \right\}$$
$$\times T_{i,j}^n + \Delta T_{1-6} \qquad (36)$$

and

$$T_{i,j}^{n+1} = \left\{ \left(\frac{k_5 - k_1}{k_1}\right) \left\langle \frac{2k_1 F_{o_1} F_{o_5}}{(k_1 F_{o_5} - k_5 F_{o_1})} \right\rangle \right\} T_{i+1,j}^n$$
$$+ \left\{ 1 + \left(\frac{k_1 - k_5}{k_1}\right) \left\langle \frac{2k_1 F_{o_1} F_{o_5}}{(k_1 F_{o_5} - k_5 F_{o_1})} \right\rangle \right\}$$
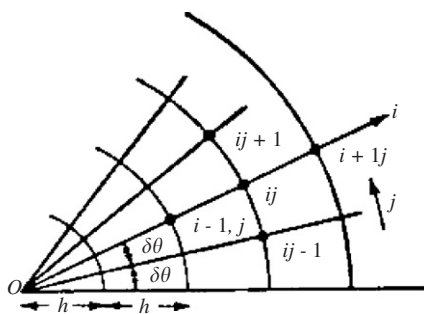$$\times T_{i,j}^n + \Delta T_{1-5}. \qquad (37)$$

Fig. 3. Discretization of extrusion chamber.

The temperature increase ΔT_{1-5} due to boundary friction in a time increment β is given by

(i) over the cylindrical part of the surface (container and undeformed billet):

$$\Delta T_{1-5} = \frac{\dot{W}_{f_c} \beta}{J \, \mathrm{Vol}(C_1 \rho_1 + C_5 \rho_5)/2},$$

where $\dot{W}_{f_c}$ is the friction power generated at billet/container interface evaluated by upper bound using surface integral. Vol the volume of billet in contact with the container.

Zone 2: Deforming region (interior nodes)

Substituting the partial differential form of Eq. (22) with the equivalent finite difference form and following through the same approach similar to that expressed by Eq. (35a) and (35b), a typical temperature distributions at point i,j within the deformation zone, assuming a square mesh, i.e. $r = \Delta r = \Delta z = i\Delta l$, gives

$$T_{i,j}^{n+1} = F_o(1 + \frac{1}{2i})T_{i+1,j}^n + F_o(1 - \frac{1}{2i})T_{i-1,j}^n,$$
$$+ (1 - 4F_o)T_{i,j}^n + (F_o - \frac{V_o \beta}{2\Delta l})T_{i,j+1}^n,$$
$$+ (F_o + \frac{V_o \beta}{2\Delta l})T_{i,j-1}^n + \Delta T_2. \qquad (38)$$

At each point in the deformation zone, ζ per cent of the deformation energy is transformed into heat, where this ζ has a value between 85% and 95% [2]. The change in temperature, ΔT_2, which is induced by plastic deformation in the time interval β, is given by

$$\Delta T_2 = \frac{\dot{W}_i}{JC\rho} \frac{\zeta}{100},$$

where J is the mechanical equivalent of heat 4185 J/kcal and $\dot{W}_i$ the power of plastic deformation /unit volume evaluated by upper bound method of analysis using volume integral.

Now, replacing the partial differential form of Eqs. (23) and (24), representing the energy balances between the undeformed billet/deforming billet and the deforming billet/extrude interfaces, with the equivalent finite difference form to give the next expressions representing the temperature distributions at respective interfaces, assuming, $\Delta z = \Delta l$, as

$$T_{i,j}^{n+1} = \frac{2\beta}{(\rho_1 C_1 - \rho_2 C_2)\Delta l}$$
$$\times \left\{ k_2 \frac{(T_{i,j+1}^n - T_{i,j}^n)}{\Delta l} - k_1 \frac{T_{i,j+1}^n - T_{i,j}^n}{\Delta l} \right\}$$
$$+ T_{i,j}^n + \Delta T_j \qquad (39)$$

and

$$T_{i,j}^{n+1} = \frac{2\beta}{(\rho_2 C_2 - \rho_3 C_3)\Delta l}$$
$$\times \left\{ k_3 \frac{(T_{i,j+1}^n - T_{i,j}^n)}{\Delta l} - K_2 \frac{T_{i,j+1}^n - T_{i,j}^n}{\Delta l} \right\}$$
$$+ T_{i,j}^n + \Delta T_j. \tag{40}$$

Since deforming billet/undeformed billet and the deforming billet/extruded billet is still the same material, it can be assumed that the density, ρ, heat capacity, C, and even thermal conductivity, K, remain constant for the material under consideration in this analysis. The typical finite difference representation of temperature distribution at any of these interfaces is given by

$$T_{i,j}^{n+1} = 2F_o T_{i,j+1}^n + (1 - 4F_o)T_{i,j}^n + 2F_o T_{i,j-1}^n + \Delta T_j. \tag{41}$$

Deforming region (boundary nodes)

Using Taylor's series expansion, the temperature distribution along the irregular boundaries is obtained by substituting the derived finite difference equivalent of partial differential Eq. (19) gives

$$T_{i,j}^{n+1} = \left(\frac{2F_o}{F(1+F)} + \frac{F_o}{2i}\right)T_{i+F\Delta r,j}^n$$
$$+ \left(\frac{2F_o}{(1+F)} - \frac{F_o.F^2}{2i}\right)T_{i-1,j}^n$$
$$+ \left(1 - \frac{2F_o}{F} - \frac{2F_o}{G}\right)T_{i,j}^n + \Delta T_{2-4}$$
$$+ \left(\frac{2F_o}{G(1+G)} - \frac{V_o\beta}{2G(1+G)\Delta l}\right)T_{i,j-G\Delta l}^n$$
$$+ \left(\frac{2F_o}{G(1+G)} - \frac{V_o\beta}{2G(1+G)\Delta l}\right)T_{i,j+1}^n, \tag{42}$$

where F and G are factors used to adjust nodes at irregular boundaries.

ΔT_{2-4} = temperature change due to internally generated heat due to frictional effect, internal power of deformation and heat resulting from velocity discontinuities; this is obtained using upper bound as $\Delta T_{2-4} = \Delta T_2 + \Delta T^*$ where ΔT_2 is the change in temperature resulting from plastic deformation and ΔT^* the change in temperature due to boundary frictional power at the deforming billet/die interface.

The expression for the heat transfer governing equation across the boundary of the deforming billet and the die is given, assuming a square grid network, as

$$T_{i,j}^{n+1} = \left\{ \frac{2k_4 F_{o_2} F_{o_4}}{(k_2 F_{o_4} - k_4 F_{o_2})} \right\}$$
$$\times T_{i+1,j}^n \left\langle \frac{2k_2 F_{o_2} F_{o_4}}{(1+F)(k_2 F_{o_4} - k_4 F_{o_2})} \right\rangle T_{i+F\Delta l,j}^n$$
$$+ \left\{ 1 + \frac{2F^2 k_2 F_{o_2} F_{o_4}}{(1+F)(k_2 F_{o_4} - k_4 F_{o_2})} - \frac{2k_4 F_{o_2} F_{o_4}}{(k_2 F_{o_4} - k_4 F_{o_2})} \right\}$$
$$\times T_{i,j}^n + \Delta T_{2-4}, \tag{43}$$

where

$$\Delta T_{2-4} = \frac{\dot{W}_i}{JC\rho} \frac{\zeta}{100} + \frac{\dot{W}_{f_d}\beta}{J(C_2\rho_2 V_2 + C_4\rho_4 V_4)/2},$$

where J is the mechanical equivalent of heat 4185 J/kcal, V_2, V_4 the volume of the billet and die region, respectively, $\dot{W}_{f_l}$ the frictional power of plastic deformation /unit volume evaluated by upper bound method of analysis using volume integral, and $\dot{W}_{f_d}$ the friction power generated over the die surface evaluated by upper bound using surface integral.

Also, the heat conducted into the die region will eventually be dissipated into the surrounding which is made up of heat conducted to grid point added to the change in the internal energy of the die at the grid point bordering with the ambient:

$$T_{i,j}^{n+1} = (1 + 2F_o + 2BiF_o)T_{i,j}^n - 2F_o(T_{i+1,j}^n + BiT_\infty). \tag{44}$$

$F_o = \alpha\beta/(\Delta l)^2$ is the finite difference representation of Fourier number and $Bi = h^*\Delta l/K$ is the finite difference representation of Biot number.

Zone 3: Extruded section

Substituting the partial differential form of Eq. (28) with the equivalent finite difference form, the temperature distribution at any point within the undeformed billet assuming a square mesh points, i.e. $\Delta r = \Delta z = \Delta l$, gives

$$T_{i,j}^{n+1} = F_o\left(1 + \frac{1}{2i}\right)T_{i+1,j}^n + F_o\left(1 - \frac{1}{2i}\right)T_{i-1,j}^n$$
$$+ (1 - 4F_o)T_{i,j}^n + \left(F_o - \frac{V_o\beta}{2\Delta l}\right)T_{i,j+1}^n$$
$$+ \left(F_o + \frac{V_o\beta}{2\Delta l}\right)T_{i,j-1}^n + \Delta T_6. \tag{45}$$

ΔT_6 = temperature change due to heat generated by frictional ironing at die land and is expressed as

$$\Delta T_{3-amb} = \frac{\dot{W}_{f_l}\beta}{J(C_3\rho_3 V_3 + C_c\rho_c V_c)/2},$$

where $\dot{W}_{f_l}$ is the friction power generated over the die land length evaluated by upper bound using surface integral and V_3, V_c the volume of the billet and container (die land housing), respectively.

The energy balance between the extruded portion and the surrounding in the finite difference is given as

$$T_{i,j}^{n+1} = (1 + 2F_o + 2BiF_o)T_{i,j}^n - 2F_o(T_{i+1,j}^n + BiT_\infty). \tag{46}$$

Zone 4: Die

Substituting the partial differential form of Eq. (29) with the equivalent finite difference form, the temperature distributions at any point within the die, assuming a square

grid or mesh points, i.e. $\Delta r = \Delta z = \Delta l$, gives

$$T_{i,j}^{n+1} = F_o(1 + \frac{1}{2i})T_{i+1,j}^n + F_o(1 - \frac{1}{2i})T_{i-1,j}^n$$
$$+ (1 - 4F_o)T_{i,j}^n + (F_o - \frac{V_o\beta}{2\Delta l})T_{i,j+1}^n$$
$$+ (F_o + \frac{V_o\beta}{2\Delta l})T_{i,j-1}^n. \tag{47}$$

The finite difference of the equation representing the energy balance between the die and the ambient is given as

$$T_{i,j}^{n+1} = (1 + 2F_o + 2BiF_o)T_{i,j}^n - 2F_o(T_{i+1,j}^n + BiT_\infty). \tag{48}$$

Zone 5: Container

Substituting the partial differential form of Eq. (31) with the equivalent finite difference form, the temperature distributions at any point within the container, assuming a square grid or mesh points, i.e. $\Delta r = \Delta z = \Delta l$, gives

$$T_{i,j}^{n+1} = F_o(1 + \frac{1}{2i})T_{i+1,j}^n + F_o(1 - \frac{1}{2i})T_{i-1,j}^n$$
$$+ (1 - 4F_o)T_{i,j}^n + (F_o - \frac{V_o\beta}{2\Delta l})T_{i,j+1}^n$$
$$+ (F_o + \frac{V_o\beta}{2\Delta l})T_{i,j-1}^n. \tag{49}$$

The finite difference of the equation representing the energy balance between the container and the ambient is given as

$$T_{i,j}^{n+1} = (1 + 2F_o + 2BiF_o)T_{i,j}^n - 2F_o(T_{i+1,j}^n + BiT_\infty). \tag{50}$$

Zone 6: Punch

Substituting the partial differential form of Eq. (33) with the equivalent finite difference form, the temperature distribution at any point within the punch, assuming a square grid or mesh points, i.e. $\Delta r = \Delta z = \Delta l$, gives

$$T_{i,j}^{n+1} = F_o(1 + \frac{1}{2i})T_{i+1,j}^n + F_o(1 - \frac{1}{2i})T_{i-1,j}^n$$
$$+ (1 - 4F_o)T_{i,j}^n + (F_o - \frac{V_o\beta}{2\Delta l})T_{i,j+1}^n$$
$$+ (F_o + \frac{V_o\beta}{2\Delta l})T_{i,j-1}^n. \tag{51}$$

The finite difference form of heat lost to the surrounding through the rear end is made up of heat conducted to the interface between the pad and billet added to the change in the internal energy of the pad at the interface is given as

$$T_{i,j}^{n+1} = (1 + 2F_o + 2BiF_o)T_{i,j}^n - 2F_o(T_{i+1,j}^n + BiT_\infty). \tag{52}$$

2.4. Stability analysis

This is concerned with the conditions that must be satisfied, if the solution of the finite difference equation is to be a reasonably accurate approximation to the solution of the corresponding partial differential equation.

These conditions are associated with two different, but interrelated problems. The first concerns the convergence of the exact solution of the differential, the second concerns

the unbounded growth or controlled decay of any errors associated with the solution of the finite difference equations, stability has been shown [11–14], to be a necessary and sufficient condition for convergence.

For stability, the coefficient of $T_{i,j}^n$ must contribute positively to growth of temperature, $T_{i,j}^n$, i.e. the coefficient in each of the equations must be greater than zero, if the coefficient of $T_{i,j}^n$ is negative it can lead to instability in values of temperature $T_{i,j}^{n+1}$ as computation is repeated for successive spatial step in time.

Now, for stability of the difference Eqs. (35), (38), (45), (47), (49) and (51) representing the temperature distribution within the homogeneous nodes, we have

$$1 - 4F_o \geqslant 0, \tag{53}$$

from which we have

$$F_o \leqslant \frac{1}{4}. \tag{54}$$

For stability of the boundary Eq. (37), we have

$$1 + \left(\frac{k_1 - k_5}{k_1}\right)\left\langle\frac{2k_1F_{o_1}F_{o_5}}{(k_1F_{o_5} - k_5F_{o_1})}\right\rangle \geqslant 0, \tag{55}$$

from which

$$\frac{k_1F_{o_1}F_{o_5}}{(k_2F_{o_3} - k_3F_{o_2})} \leqslant \frac{k_1}{2(k_1 - k_5)}. \tag{56}$$

For stability of the boundary Eq. (36), we have

$$1 + \left(\frac{k_1 - k_6}{k_1}\right)\left\langle\frac{2k_1F_{o_1}F_{o_6}}{(k_1F_{o_6} - k_6F_{o_1})}\right\rangle \geqslant 0, \tag{57}$$

from which

$$\frac{k_1F_{o_1}F_{o_6}}{(k_1F_{o_6} - k_6F_{o_1})} \leqslant \frac{k_1}{2(k_1 - k_6)}. \tag{58}$$

For the stability of heat lost to the ambient (Eqs. (41), (44), (46), (48), (50) and (52)), we have

$$1 + 2F_o + 2BiF_o \geqslant 0, \tag{59}$$

from which

$$F_o = \frac{1}{2(1 + Bi)}.$$

For Eq. (40), which represents the node at irregular boundary, to be numerically stable we have

$$1 + \frac{2F_o}{F} + \frac{2F_o}{G} \geqslant 0, \tag{60}$$

from which

$$F_o \leqslant \frac{FG}{2(G + F)}.$$

Note that $FG/2(G + F)$ will be equal to $\frac{1}{4}$ when $F = G = 1$ representing the stability criterion for regular nodes.

For Eq. (41) (see Eq. (51)) to be numerically stable:

$$1 + \frac{2F^2k_2F_{o_2}F_{o_4}}{(1 + F)(k_2F_{o_4} - k_4F_{o_2})} - \frac{2k_4F_{o_2}F_{o_4}}{(k_2F_{o_4} - k_4F_{o_2})} \geqslant 0,$$

from where

$$\frac{F_{o_2} F_{o_4}}{(k_2 F_{o_2} - k_4 F_{o_2})} \leqslant \frac{1 + F}{2 F^2 (k_2 - k_4)}. \tag{61}$$

The minimum allowable value of time spatial step in size, $(\beta,)$ is then obtained from F_o using the relation, $\beta = F_o \Delta l^2 / \alpha$ which was then used for computation.

2.5. Computational methods

2.5.1. Description of computer programme and application

During the extrusion, heat is generated by deformation and boundary friction. Conduction takes place while the heat sources, i.e. the deformation of the volume elements within the deformation zone and boundary friction due to the descent or movement of punch, is according to the velocity fields postulated. In order to analyze this problem, it is necessary to approximate the deformation in a time increment β with conduction taking place simultaneously. The minimum value of β is determined from the stability conditions (Eqs. (51)–(59)) in the heat conduction equations, since none of the coefficients of T_{ij} should be negative. Assuming that the entire heat generation takes place during the motion of a point from its initial position to an instantaneous point in time β, the additional temperature increases due to rate of plastic deformation work, ΔT_4, rates of work due to boundary friction at undeformed billet/container, ΔT_{2-3} and die land, ΔT_6 are calculated using appropriate expressions. Using the calculated ΔT values, which include the increases due to plastic deformation and boundary friction, the heat flow equations are analyzed and the temperature distribution in the time interval β is determined.

The computer program written in C++ language essentially simulates the extrusion process and takes into account the motion of the billet–punch interface. It is obvious that the temperature distributions in the extruded material during extrusion depends on several factors such as material properties, friction conditions, ram velocity, extrusion ratio, preheat die temperature, billet height, and die land length. All these variables are taken into account in the computer program.

3. Experimental procedure

3.1. Specimen preparation

The lead alloy workpieces of approximate percentage compositions of Zn (3.50%), Pb (96.47%), Cd (0.0032%), Ni (0.0033%), and Cu (0.02%) was obtained from the lead ingot put in a crucible and melted in an electric furnace before casting them into already prepared sand moulds. The cast lead alloys of dimension 45 mm in diameter were machined into smaller lead alloy workpieces of dimensions 39 mm in diameter by 26 mm and 22 mm in height. Concentric grooves were made on the diametrical ends of
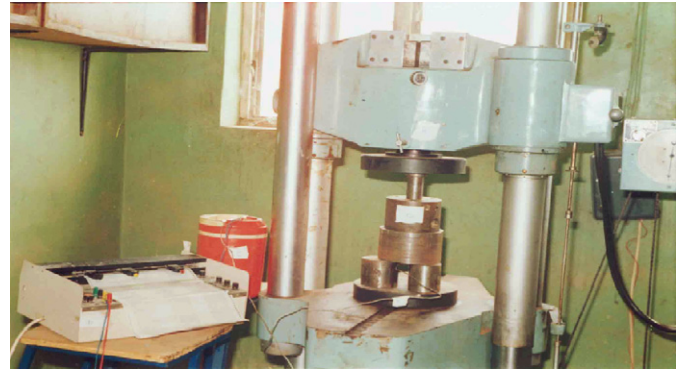

Fig. 4. Temperature monitoring set-up.

the billets, so as to facilitate the retention of lubricant during extrusion process.

3.2. Extrusion and temperature measurements

The container walls, dies, punch, and specimen were first cleansed with methylated spirit solution to remove any grease from them, and they were then lubricated with shear butter for each test. Thermocouple (type K) was screwed into the die, until the tip appeared slightly out of the die surface. The whole die assembly with thermocouple in position was then screwed into the housing or container and the extrusion rig centrally placed on the hydraulic press. The hot workpiece taken from the electric furnace was, however, dropped into the extrusion chamber at an initial temperature of 70 °C. The thermocouple leads were connected to the chart recorder through cold junction container with melting ice at 0 °C to indicate the room temperature and the billet's temperatures in the extrusion container. The chart recorder plotted the temperature versus time curve, as the extrusion process progressed. The extrusion speed used was 0.05 mm/s throughout the extrusion process. The experiment was stopped at the steady stage of the extrusion process (Fig. 4).

4. Results and discussion

4.1. Percentage reduction in area and billet heights on extrusion temperatures

Fig. 5(a) and (b) show, respectively, the effect of billet heights on the experimental and theoretical comparisons of the temperature rise distributions during the extrusion of lead alloy at the die surface or within the dead metal zone at percentage reduction in area of 95%. The theoretical and experimental temperature rises, respectively, to peak temperatures of 66.10, 65.6, and 61.3 °C, 60.50 °C for billet's heights of 26 and 22 mm, respectively. These peak temperatures, respectively, fall to constant steady-state theoretical values of 62.56, 62.16 °C and steady-state experimental values of 46.5, 45 °C for respective billet's heights of 26 and 22 mm (see Table 1).
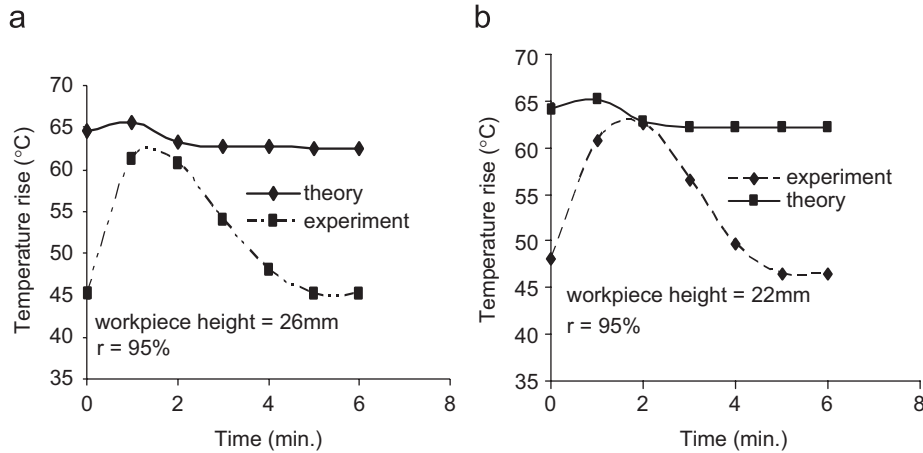
Fig. 5. Experimental and theoretical comparison of the effects of workpiece height, Ho, on the temperature rise during the forward extrusion of lead alloy.

Fig. 6(a) and (b) show comparisons of the experimental and theoretical variations in temperature at reductions in area of 95% and 85% at a given punch speed of 0.05 mm/s and a workpiece height of 26 mm. The temperature versus time curves rise initially to different peak temperatures, depending on the reductions in areas and later drop to a minimum constant temperatures after about 4 min of the extrusion process, to the stop of extrusion process. The peak temperatures attained in all these curves were lower than the initial billet's temperature of 70 °C due to chilling effect, as a result of lower mode temperature of extrusion container's walls. The effect of reduction in area on temperature rise during extrusion process is clearly seen in the plots. Increasing percentage reduction shows increasing temperature rise. The theoretical and experimental temperature rises, respectively, to peak temperatures of 66.10 and 64.3, and 62.5 and 55.2 °C for percentage reductions in areas of 95% and 85%. These peak temperatures, respectively, fall to constant steady-state theoretical values of 62.6 and 61.0 °C and steady-state experimental values of 45.3 and 40.5 °C for percentage reduction in area of 95% and 85% (see Table 2).

It is seen, from Figs. 5 and 6 that the measured and calculated temperatures agree fairly well (especially the peak values) for the two cases but it should be noted that the calculated values are higher than the measured values. This is expected as upper bound is expected to give over estimated temperature rise. The maximum difference between the measured and calculated temperature rise being 8.7 °C for percentage reduction in area and 4.7 °C for billet height at the peak temperature, while the steady-state maximum difference being 18.4 °C for percentage reduction in area and also for billet height. The temperature differences between theory and practical results can be explained as due to the following.

(i) The thermal inertia of the thermocouple makes its response to temperature changes to be slow at the early stage of extrusion process.

Tables 1
Effect of billet height on the peak temperatures in forward extrusion with initial billet temperature of 70 °C and reduction ratio of 95%

Billet height (mm)	Peak temperature (°C)		Steady-state temperature (°C)	
	Experiment	Theory	Experiment	Theory
22	60.5	65.24	45.0	62.16
26	61.25	65.66	46.5	62.56

(ii) The assumption of billet making an instant perfect contact with the container is not completely true, as there exists small gaps between the warm billet and the container wall which allows some convection heat transfer to take place throughout the compression stage of extrusion that is not accounted for in this analysis.
(iii) The heat generated was evaluated using kinematically admissible velocity fields based on upper bound method of analysis which normally is expected to give temperature higher than the actual value.

4.2. Extrusion speed and percentage reduction in area on extrusion temperature

Figs. 7 and 8 show the effect of extrusion speeds at the dead metal zone and the die land zone on the temperature rise with punch displacement during the extrusion of lead alloy. In each case, an initial rise in temperature followed by a more gradual rise in the temperature occurs during the extrusion process. It can be observed that, the temperature first fall below the initial billet temperature of 70 °C apparently due to the container/tool chilling effect. The initial temperature rise at dead zone is found to be lower than that of the die land, because at the die land region more heat has been generated due to frictional ironing work being converted to heat leading to a gradual rise above the dead zone temperature rise. However, as the extrusion speed increases, we see (Fig. 9) that the rate of
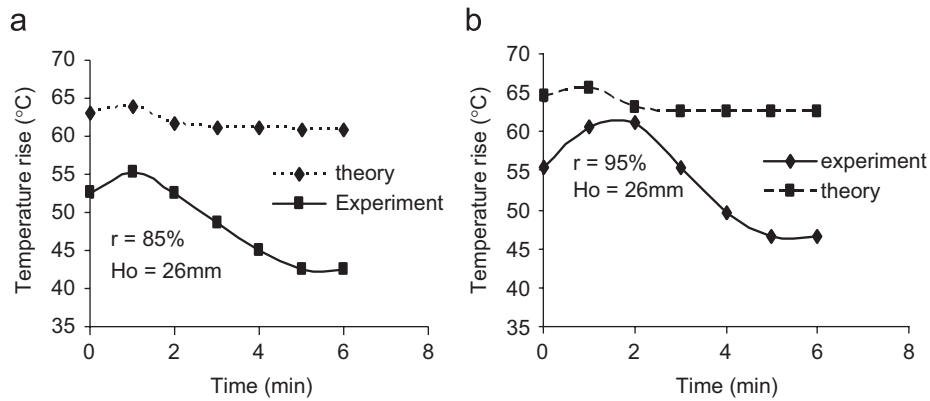
Fig. 6. Experimental and theoretical comparison of the effects of percentage reductions in area, *r* on the temperature rise during the forward extrusion of lead alloy: (a) experimental and (b) theory.

Tables 2
Effect of reduction ratio on the peak temperatures in forward extrusion with initial billet temperature of 70 °C and initial billet height of 26 mm

%*r*	Peak temperature (°C)		Steady-state temperature (°C)	
	Experiment	Theory	Experiment	Theory
85	55.25	63.97	42.5	60.93
95	61.25	65.66	46.5	62.56
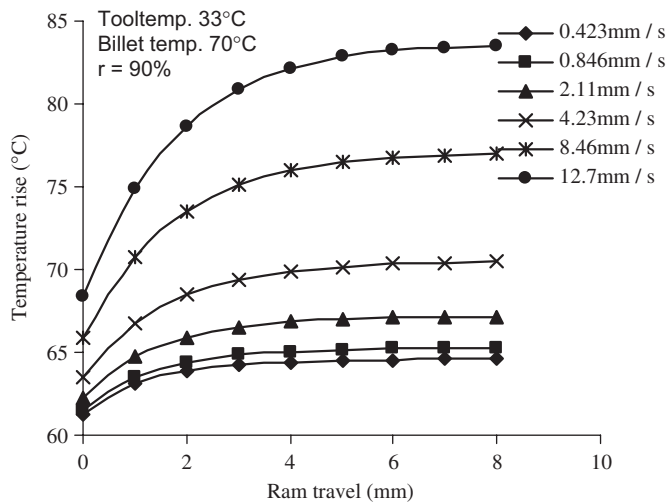
Fig. 7. The effect of extrusion speed on temperature rise at dead metal zone (DMZ) during direct extrusion of lead alloy.

Fig. 8. The effect of extrusion speed on the temperature rise at die land zone (DLZ) during the extrusion of lead alloy.

temperature rise is faster at the dead metal zone than at extrude or die land position. This shows that more heat flows into the dead metal zone due to internal heat generated as a result of increasing plastic power of deformation and power due to velocity discontinuities than that generated at die land zone due to frictional work being converted to heat. This is the result of the direct and wider contact area of this zone with the main deformation zone as well as the great amount of heat flowing into it and emitted in this zone during conversion of the deformation work into heat. This is in agreement with Singer and
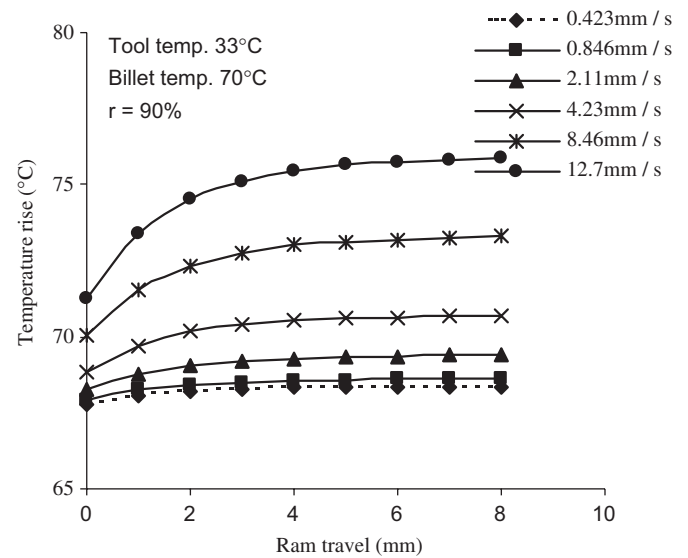
Al-Samarrai [5] that changes in speeds are followed by more gradual changes in emergent temperatures. Also, Sheppard and Raybould [15] asserted that the dead metal zone temperature rise is always higher than any other position considered during extrusion. In the present investigation, the extrusion speeds below 4.23 mm/s have the die land zone temperature rise, show higher temperature rises than that of the dead zone. However, beyond this extrusion speed, dead zone shows speedy rises in temperature than that of the die land zone with increasing extrusion speeds. This should be because of the higher intensity of heat generated at the main deformation zone flowing to this dead metal zone portion.

Fig. 10 shows the relationship between temperature rise at dead metal zone with percentage reduction in areas. We can see that below percentage reduction in area of 90%, the heat or temperature rise at the dead metal zone is lower than that at the die land zone. This can be explained that at lower percentage reduction not much deformation work is converted into heat at the main deformation zone, and
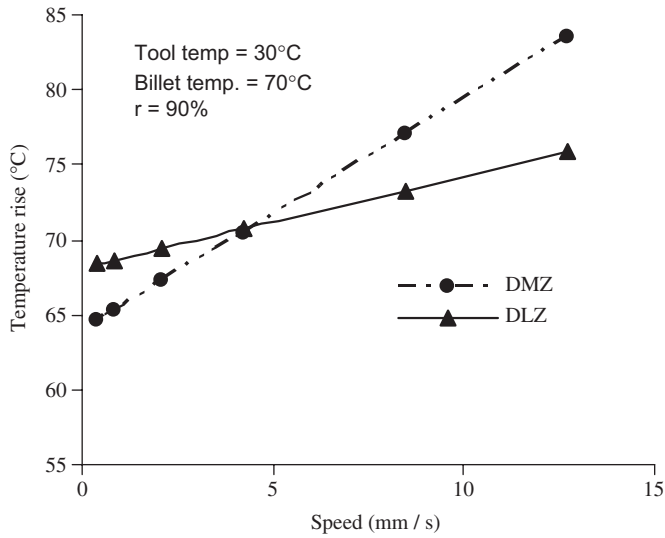
Fig. 9. The effect of speed on temperature rise at the dead metal zone (DMZ) and die land zone (DLZ) during the extrusion of lead alloy.
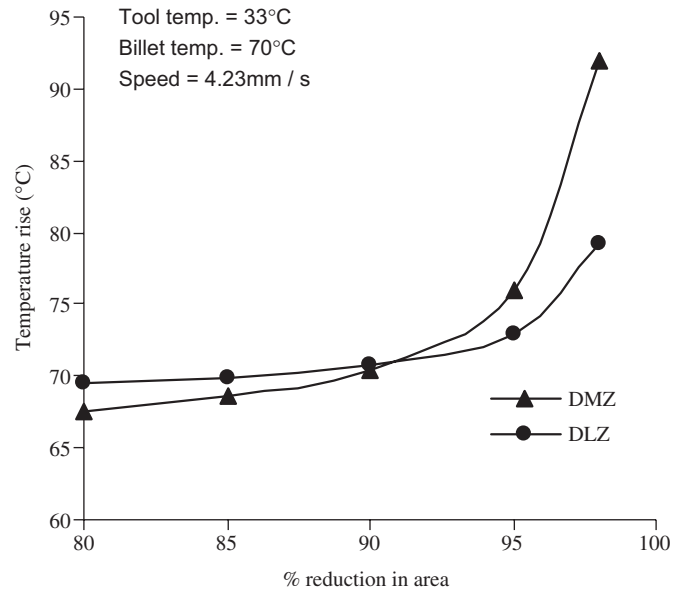
consequently not much heat is emitted into the dead metal zone, unlike the direct contact and conversion of frictional work into heat at die land zone, leading to direct but gradual rise in temperature. But as percentage reduction in area increases, especially beyond 90%, it leads to increase in extrusion temperature. This can be further explained by the fact that the energy needed to deform the material increases, so does the deformation work which converts into heat in the main deformation zone.

Figs. 11 and 12 show the effect of tool temperature and billet temperatures on the temperature rise during extrusion process. A steady rise in temperature is noticed with increasing percentage reduction in area till a critical percentage reduction of 90% when a sudden temperature rise is noticed for the two tool temperatures considered. It can be seen that higher tool temperature gives higher extrusion temperature at the dead metal zone (see Fig. 11). The steady rise in the extrusion temperature in Fig. 12 tends to continue till percentage reduction in area of 95% before a sudden rise in temperature is observed and this is because at higher billet temperature the flow stress of the material is reduced. Also, it can be seen that the higher the billet temperature the higher will be the extrusion temperature rise.

4.3. Initial tool/container and billet temperatures on extrusion temperature rise

Figs. 13 and 14 show that the temperature rises sharply at the die land zone and at the dead metal zone, respectively, during the first stage of extrusion followed by a more gradual rise in temperature. The plots show the effects of initial tool temperature on the temperature rises with ram travel at the die land zone and at dead metal zone during extrusion process. Generally, for the extrusion speeds considered, the extrusion temperature rises are seen

Fig. 10. Relationship between temperature rise at dead metal zone (DMZ) and die land zone (DLZ) with varying percentage reduction in area during extrusion of lead alloy.
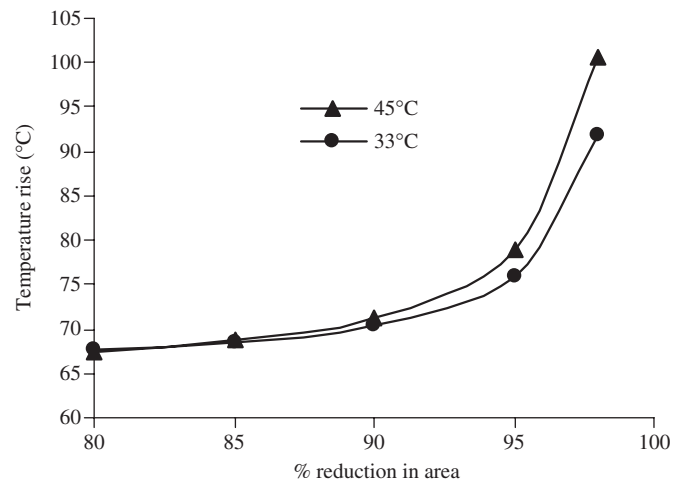

Fig. 11. Effect of tool preheat temperature on temperature rise at dead metal zone (DMZ) with varying percentage reduction in area in direct extrusion of lead alloy.

to be lower with lower container temperature at both positions (see Figs. 13 and 14). The effect of tool temperature is, however, seen to be more pronounced at the dead metal zone than at the die land zone. It can be further seen that at both positions, the higher the speed the more pronounced the effect of initial container temperature on the temperature rises become (see Fig. 15).

A similar trend is observed, while analyzing the effect of the billet temperatures on the extrusion temperature changes (see Fig. 12). Maintaining the same tool/container temperature, it is obvious that the extrusion temperature increases with the initial temperature of the billet. A gradual change is observed with increasing percentage

reduction in area till about 95%. Beyond this, a shaper rise in temperature is observed at the dead metal zone for both tool/container temperatures investigated. This is due to additional work needed to overcome resistance posed by the tooling which also resulted into additional heat generated.

4.4. Friction coefficients on extrusion temperatures

Fig. 16 is the plot of temperature rise at the dead metal zone and at the die land zone versus friction coefficient. The die land zone shows increasing temperature rise with increasing friction coefficient, while increasing friction

coefficient has no effect on the dead metal zone temperature rise. This finding is consistent with Watkins et al.'s [16] assumption of ignoring friction at deformation zone because friction has no overall effect on the temperature rise in the deformation zone since its effect will mainly be surface effects that are compensated for by a drop in yield stress.

5. Conclusion

It is found both experimentally and theoretically that for a given percentage reduction in area, the temperature rise is slightly higher for higher initial billet height, and the higher the percentage reduction in area, the higher the temperature rises during the extrusion process. This could be explained by the fact that the energy needed to deform the material increases, so does the deformation work as well as frictional work, especially at the die land zone, which converts itself into heat in the main deformation zone and die land zone. The dead zone temperature generally rises sharply more than the die zone temperature essentially beyond 90% reduction in area. This is due to direct and wider contact area of this zone with the main deformation zone as well as of great amount of heat flowing into it and emitted in this zone during conversion of the deformation work into heat. Increasing coefficient of friction shows increase extrusion temperature at the die land zone and shows no significant rise in extrusion temperature at the dead zone. However, increasing speed of deformation shows a greater dead zone temperature rise than a more gradual die land temperature rise beyond an extrusion speed of 4.23 mm/s. Generally, increasing speed leads to increasing temperature rise.
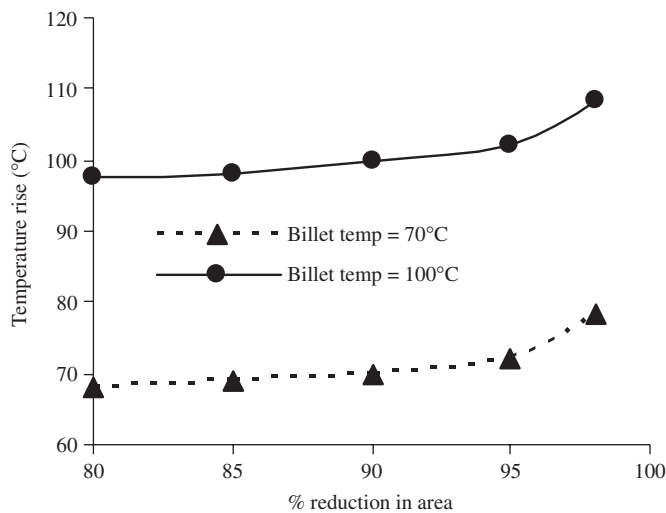

Fig. 12. Effect of billet preheat temperature on temperature rise at die land zone (DLZ) with varying percentage reduction in area during extrusion of lead alloy.
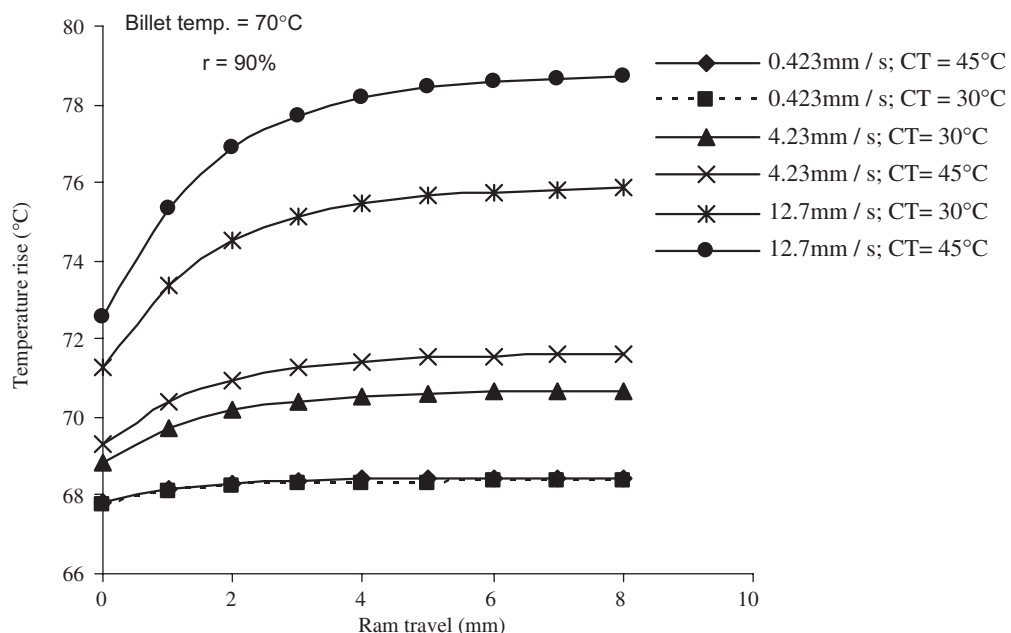

Fig. 13. The effect of extrusion speed on temperature rise at the die land zone (DLZ) during extrusion of lead alloy.
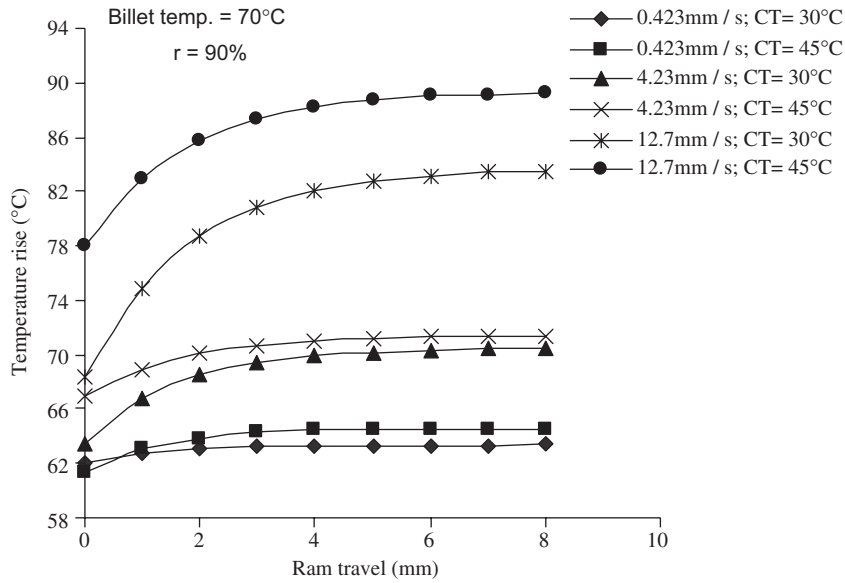
Fig. 14. The effect of extrusion speed on temperature rise at the dead metal zone (DMZ) during extrusion of lead alloy.
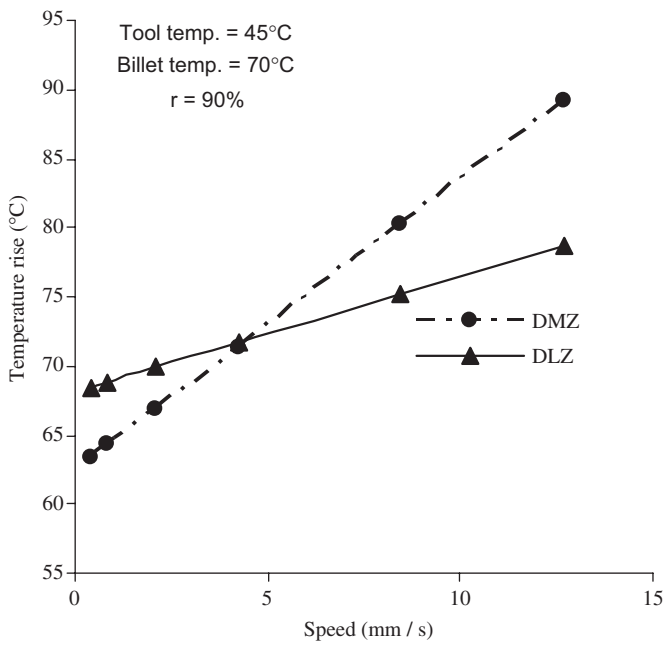

Fig. 15. The effect of extrusion speed on the temperature rise at the dead metal zone (DMZ) and die land zone (DLZ) during the extrusion of lead alloy.
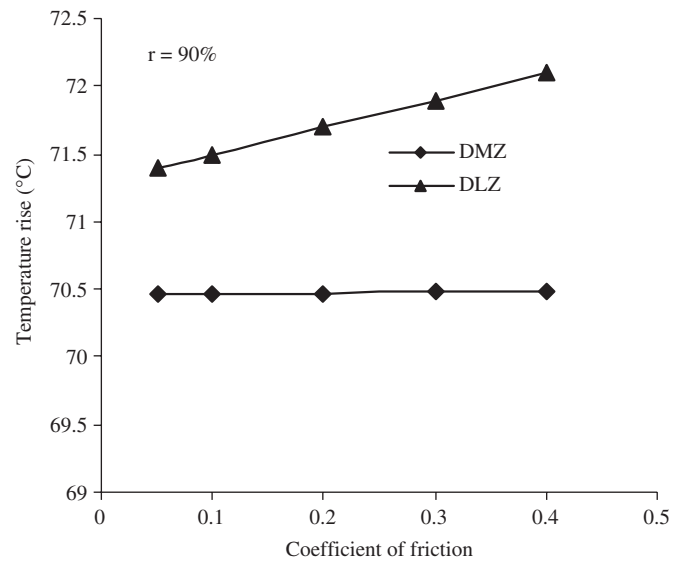

Fig. 16. The effect of friction coefficient on the temperature rise at the dead metal zone (DMZ) and die land zone (DLZ) during extrusion of lead alloy.

Reference

[1] Farren WS, Taylor GI. The heat developed during plastic extrusion of metals. Proceedings of the Royal Society, Series A 1925;107:422.
[2] Altan T, Kobayashi S. A numerical method for estimating the temperature distributions in extrusion through conical dies. Journal of Engineering for Industry (Transactions of the ASME) 1968: 107–18.
[3] Akeret R. A numerical analysis of temperature distribution in extrusion. Journal of the Institute of Metals 1967;95:204–11.
[4] Tanner RI, Johnson W. Temperature distribution in the die zone during fast extrusion operations. International Journal of Mechanical Sciences 1960;1:28.

[5] Singer ARE, Al-Samarrai SHK. Temperature changes associated with speed variation during extrusion. Journal of the Institute of Metals 1961;89:225–31.

[6] Johnson W, Kudo H. The use of upper-bound solutions for the determination of temperature distributions in fast hot rolling and axisymmetric extrusion processes. Journal of the Mechanical Sciences 1960;1:175.

[7] Kiuchi M, Kish H, Ishikawa M, Study on Non symmetric extrusion and drawing, International Journal of Machine Tool, Design and Research conference, 22nd proceedings, 1981. p. 523–32.

[8] Ajiboye JS, Adeyemi MB. Upper bound analysis for extrusion at various die land lengths and shaped profiles. International Journal of Mechanical Sciences 2007;49:335–51.

[9] Ajiboye JS, Extrusion pressure and temperature changes during forward extrusion process. PhD thesis, Department of Mechanical Engineering, University of Ilorin, Nigeria, 2006.

[10] Kim NH, et al. Die design optimization for axisymmetric hot extrusion of metal matrix composites. International Journal of Mechanical Science 2001;43:1507–20.

[11] Smith JD. Numerical solution of partial differential equations: finite difference method (FDM). 2nd ed. Oxford: Clarendon Press; 1978.

[12] Cengel YA. Heat and mass transfer: a practical approach. 3rd ed. New York: McGraw-Hill; 2006.

[13] Hastaoglue MA. Numerical solution of three dimensional moving boundary problems: melting and solidification with blanketing of a third layer. Chemical Engineering Science 1987;45(10):2417–23.

[14] Ozisik MN. Basic heat transfer. New York: McGraw-Hill Book Company; 1977.

[15] Sheppard T, Raybould D. On load and temperature rise during the extrusion of superpure Al, Al–Zn, and AI–Zn mg alloys. Journal of the Institute of Metals 1973;101:33–44.

[16] Watkins MT, et al. Mechanical Engineering Research Laboratory (Plasticity Division) Report 102 1954.